

Analysis of spherical indentation of linear viscoelastic materials

M. V. Ramesh Kumar¹ and R. Narasimhan^{2,*}

¹Armament Research and Development Establishment, Pune 411 021, India

²Department of Mechanical Engineering, Indian Institute of Science, Bangalore 560 012, India

In this article, the time-dependent spherical indentation response of a linear, isotropic, viscoelastic material to different load histories is studied. To this end, finite element computations and depth-sensing micro-indentation experiments using polymethyl methacrylate specimens are undertaken. The validity of viscoelastic indentation theories is assessed by comparing with the finite element and experimental results. Finally, the creep response function is extracted from the experimentally recorded indentation displacement histories and is compared with that obtained from a conventional mechanical test. It is shown that accurate characterization of viscoelastic response of materials is possible from depth-sensing indentation, which has potential applications to components with small size scales such as thin films and biological tissues.

VISCOELASTIC materials exhibit features which combine those of elastic solids and viscous fluids¹. Thus, when a viscoelastic material is subjected to constant stress, the strain slowly increases with time, which is called as creep. On the other hand, under constant strain, the stress gradually decreases with time (i.e. the material relaxes). A variety of materials such as soils, polymers, biological tissues and cartilages display viscoelastic response. This behaviour in polymers, which can undergo large viscoelastic strains (say, up to 0.05) before deforming plastically, has been extensively studied. It is generally assumed from an analytical standpoint that the viscoelastic response is linear, which implies that it must show both linear scaling and superposition¹. The latter leads to stress versus strain relationship in terms of hereditary integrals that typically involve the creep or relaxation response function.

The viscoelastic response functions can be obtained for bulk materials by performing conventional creep or relaxation tests. They involve precise specimen preparation confining to relevant standards, accurate control of experimental parameters and testing of a number of such specimens in order to obtain reliable results (see, for example, Lu *et al.*²). However, it is impossible to conduct these tests when the sample size is small like in the case of thin films, MEMS components or biomaterials like tis-

ues. Hence, depth-sensing micro- or nano-indentation is being explored in recent years as a possible experimental technique for determining the creep or relaxation response function of viscoelastic materials³⁻⁵. In this context, it must be mentioned that the above technique has been extensively used to measure properties such as Young's modulus and hardness of materials that show time-independent behaviour⁶⁻⁸. However, application of this technique to viscoelastic materials can lead to large errors in mechanical properties^{3,5}. Hence, there is a need to develop the depth-sensing indentation procedure for characterizing the time-dependent behaviour of these materials. This requires a thorough understanding of the mechanics of contact of viscoelastic bodies.

The solution to a quasi-static boundary value problem involving a linear, isotropic viscoelastic body is generally obtained using the correspondence principle¹. However, this principle breaks down under certain situations, such as during indentation by a curved or pointed indenter. Lee and Radok⁹ obtained expressions for contact load and pressure distribution during spherical indentation of a linear viscoelastic material by replacing the elastic modulus in the Hertz solution¹⁰ by hereditary integrals involving the relaxation response function. However, this solution was found to be invalid when the contact radius a decreases with time because negative pressure develops in the contact zone⁹. This issue was addressed by Hunter¹¹ and Ting¹². The latter suggested a method which can be applied for axisymmetric indentation with arbitrary $a(t)$.

Sakai⁴ and Lu *et al.*⁵ have recently employed the equations of Lee and Radok⁹ to obtain expressions for time variation of indentation depth, $h(t)$, corresponding to simple load histories such as ramp loading. Sakai⁴ idealized the material as a Maxwell fluid or solid, whereas a more realistic Prony series representation of the creep response function $J(t)$ was used by Lu *et al.*⁵. In the latter work, a procedure was also developed for obtaining the creep response function directly from the slope of the measured $h(t)$ curve. However, due to scatter or noise in the experimental data, accurate evaluation of dh/dt becomes difficult and may lead to large errors in $J(t)$. It must be mentioned here that the validity of the viscoelastic indentation theory enunciated by Lee and Radok⁹ and Ting¹², needs to be first carefully assessed by comparing with numerical solutions obtained, for example, by the fi-

*For correspondence. (e-mail: narasi@mecheng.iisc.ernet.in)

nite element method. This is particularly important for the unloading part of the load versus displacement curve, which is routinely employed in extracting the elastic modulus in indentation studies⁶⁻⁸. The above issue constitutes one of the main objectives of the present work. Also, the time-dependent spherical indentation response of a viscoelastic material to different load histories is studied. Finally, the accuracy of determining the creep response function from indentation displacement records is examined by conducting both conventional mechanical tests and micro-indentation experiments using polymethyl methacrylate (PMMA).

Indentation theory for viscoelastic materials

A thorough discussion of contact stress theory for linear elastic solids is given by Johnson¹⁰. The Hertz contact pressure distribution when a frictionless, rigid, spherical indenter of radius R is pressed onto a linear elastic solid is given by:

$$p_e = \frac{2E^*}{\mathbf{p}R} (a^2 - r^2)^{1/2}. \tag{1}$$

Here, the subscript e refers to the linear elastic case. Also, r is the radial coordinate measured from the indenter axis, and $E^* = E/(1 - \mathbf{n}^2)$, where E and \mathbf{n} are the Young's modulus and Poisson ratio respectively. Further, the indentation depth $h_e(t)$ is related to the contact radius and load $P(t)$ by:

$$h_e = \frac{a^2}{R} = \left(\frac{3P}{4E^*\sqrt{R}} \right)^{2/3}. \tag{2}$$

Lee and Radok⁹ extended the above equations to linear viscoelasticity by replacing the Young's modulus with hereditary integrals involving the response functions. Thus, assuming the Poisson ratio \mathbf{n} to be time-independent, eqs (1) and (2) for linear viscoelasticity become,

$$p(r, t) = \frac{2}{\mathbf{p}R(1 - \mathbf{n}^2)} \int_0^t G(t - \mathbf{x}) \frac{d}{d\mathbf{x}} (\sqrt{a^2(\mathbf{x}) - r^2}) d\mathbf{x}, \tag{3}$$

$$h^{3/2}(t) = \left(\frac{a}{\sqrt{R}} \right)^3 = C_1 \int_0^t J(t - \mathbf{x}) \frac{dP(\mathbf{x})}{d\mathbf{x}} d\mathbf{x}, \tag{4}$$

where $G(t)$ and $J(t)$ are the relaxation and creep compliance functions in uniaxial compression. These are related by¹:

$$1 = J(0)G(t) + \int_0^t G(t - s) \dot{J}(s) ds, \quad \text{or} \tag{5}$$

$$1 = G(0)J(t) + \int_0^t J(t - s) \dot{G}(s) ds. \tag{6}$$

Also, the constant C_1 is given by,

$$C_1 = \frac{3(1 - \mathbf{n}^2)}{4\sqrt{R}}. \tag{7}$$

In this work, two types of load histories, namely step loading and triangular loading are considered. Since quasi-static step loading is difficult to achieve in practice, the load is ramped to its terminal value P_0 in a finite rise time $t_r = 1$ s and thereafter held constant. Thus, the applied load history for this case (which is referred to in the sequel as ramp and hold loading) can be expressed as:

$$P(t) = \dot{P}_0 t H(t) - \dot{P}_0 (t - t_r) H(t - t_r), \tag{8}$$

where $\dot{P}_0 = P_0/t_r$ and $H(t)$ is the heaviside step function. On first considering $t \leq t_r$, eq. (4) becomes:

$$h^{3/2}(t) = C_1 \dot{P}_0 \int_0^t J(\mathbf{q}) d\mathbf{q}. \tag{9}$$

The integral on the right hand side of eq. (9) can be evaluated by assuming a Prony series representation of the creep response function $J(t)$, which is given by¹:

$$J(t) = J_0 + \sum_{i=1}^{N-1} J_i (1 - e^{-t/t_i}). \tag{10}$$

On substituting eq. (10) into eq. (9), it follows that⁵,

$$h^{3/2}(t) = C_1 \dot{P}_0 \left[\left(J_0 + \sum_{i=1}^{N-1} J_i \right) t - \sum_{i=1}^{N-1} J_i t_i (1 - e^{-t/t_i}) \right]. \tag{11}$$

Similarly, for $t > t_r$, one obtains,

$$h^{3/2}(t) = C_1 \left[\left(J_0 + \sum_{i=1}^{N-1} J_i \right) P_0 + \sum_{i=1}^{N-1} \left(\frac{P_0 t_i}{t_r} \right) (1 - e^{-t_r/t_i}) e^{-t/t_i} \right]. \tag{12}$$

In the triangular loading history, the load is ramped to a peak value of P_0 in a time t_0 and then reduced to zero at $2t_0$. It can be expressed as:

$$P(t) = \dot{P}_0 t H(t) - 2 \dot{P}_0 (t - t_0) H(t - t_0), \tag{13}$$

where $\dot{P}_0 = P_0/t_0$ represents the loading rate. Thus, for $t \leq t_0$, eq. (9) or (11) will apply. On the other hand, by differentiating eq. (9) with respect to t , it follows that,

$$J(t) = \frac{3}{2C_1} h^{1/2}(t) \frac{dh}{dP}. \quad (14)$$

Equation (14) provides one method for evaluating $J(t)$ from experimentally measured $h(t)$ or $h(P)$ curve⁵ for constant loading rate.

Next, considering the time interval $t_0 < t \leq 2t_0$, it can be shown from eqs (4) and (9) that,

$$h^{3/2}(t) = h^{3/2}(t_0) + C_1 \dot{P}_0 \left[\int_{t_0}^t J(\mathbf{q}) d\mathbf{q} - 2 \int_0^{t-t_0} J(\mathbf{q}) d\mathbf{q} \right]. \quad (15)$$

However, as will be seen later, when eq. (15) is used in conjunction with eqs (4) and (3), it gives rise to negative pressure in the contact zone and results in large errors, particularly close to complete unloading. Ting¹² addressed this issue and showed that for any prescribed $a(t)$ which increases to a peak value at t_0 and thereafter decreases, the load history $P(t)$ for $t > t_0$ is given by,

$$P(t) = \frac{4}{(1-\mathbf{n}^2)R} \int_0^{t_1(t)} G(t-\mathbf{x}) a^2(\mathbf{x}) a'(\mathbf{x}) d\mathbf{x}. \quad (16)$$

Here $t_1(t)$ is the time instant during the interval $(0, t_0)$ at which $a(t_1) = a(t)$. In the present context, since $P(t)$ is prescribed, the function $t_1(t)$ is determined from the above equation by an iterative procedure. This is then used to obtain the evolution history of the contact radius $a(t)$. Finally, the contact pressure distribution $p(r, t)$ and indentation displacement $h(t)$ are derived from the following equations given by Ting¹²:

$$p(r, t) = \frac{2}{\mathbf{p}R(1-\mathbf{n}^2)} \int_0^{t_1(t)} G(t-\mathbf{x}) \frac{d}{d\mathbf{x}} (\sqrt{(a^2(\mathbf{x})) - r^2}) d\mathbf{x}, \quad (17)$$

$$h(t) = \frac{a^2}{R} - \frac{2}{R} \int_{t_0}^t J(t-\mathbf{x}) \frac{d}{d\mathbf{x}} \int_{t_1(\mathbf{x})}^{\mathbf{x}} G(\mathbf{x}-\mathbf{h}) a(\mathbf{h}) a'(\mathbf{h}) d\mathbf{h} d\mathbf{x}. \quad (18)$$

As in the earlier development, Prony series representations of $J(t)$ and $G(t)$ can be employed to evaluate the integrals occurring in eqs (16)–(18). The validity of the above equations will be examined below, by comparing with results of finite element simulations.

Relaxation tests in uniaxial compression

Standard relaxation tests are conducted on specimens fabricated from a cast PMMA plate of thickness 25.4 mm to characterize its linear viscoelastic response. To this end, cylindrical specimens according to ASTM D695 are ma-

chined from blanks cut from the PMMA plate. These blanks are annealed before machining to eliminate effects of prior processing history. The annealing involved holding the blanks at 105°C for 2 h and then cooling to room temperature at a rate of 5°C/h in a closed air furnace. Subsequently, these blanks are machined to the dimensions of $\text{f}12.7 \times 25.4$ mm. The finished specimens are again annealed to remove any residual stresses. These specimens are subjected to relaxation tests in uniaxial compression at different initial strain levels \mathbf{e}_0 ranging between 1 and 3% on an INSTRON machine at room temperature. As a true step strain pulse is not possible to apply in practice, each of these initial strain levels is attained as a ramp in 1 s, which is then held constant for an hour. The stress relaxation response of the specimen under this strain is continuously monitored.

The relaxation response function is deduced from each test following the procedure suggested by Lee and Knauss¹³. The response curves obtained from the tests with $\mathbf{e}_0 = 1$ and 1.25% are fairly close to each other. However, as \mathbf{e}_0 increases further, this curve is found to decrease, which implies breakdown of linearity of constitutive response. Thus, the threshold of linear viscoelastic regime is taken to be a strain level of about 1%. The corresponding relaxation response function $G(t)$ is plotted against time in Figure 1. The creep response function $J(t)$ is determined by numerically solving the Volterra integral equation (eq. (5))¹. This function (represented in the form of a three-term Prony series, eq. (10)) is employed to evaluate the analytical equations for viscoelastic indentation presented above.

Indentation experiments

Indentation experiments on PMMA are conducted using a micro-indentation set-up that is designed and fabricated

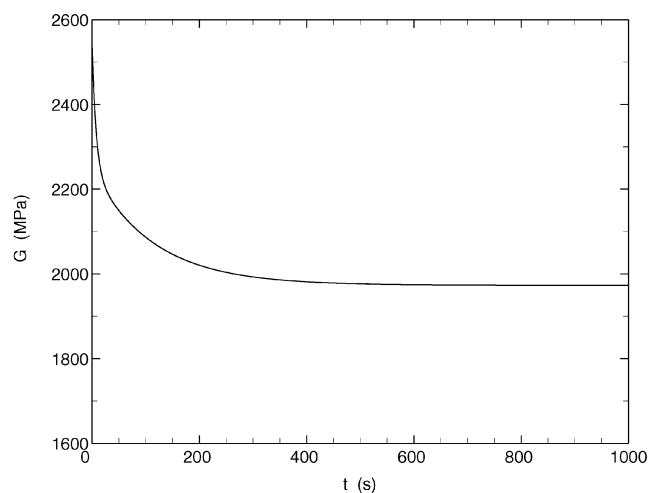


Figure 1. Relaxation response function for PMMA material considered here, determined from a conventional mechanical test.

to work in conjunction with an INSTRON machine¹⁴. This design is such that the compliance of the machine does not affect the measurements taken during indentation experiments. In addition to the mechanical attachments for assembling this set-up onto the INSTRON machine, its main elements include a spherical indenter, a load cell, an LVDT and a multichannel data-acquisition system¹⁴.

PMMA specimens for indentation experiments are fabricated from the same plate used for making the relaxation specimens. They are also subjected to the annealing cycle mentioned earlier, both before and after machining. Spherical indentation experiments (using a stainless steel indenter of radius 3.5 mm) are then conducted at room temperature by subjecting the specimens to ramp and hold, and triangular load histories. The former (with rise time $t_r = 1$ s) closely approximates step loading, while in the latter, three values of $t_0 = 10, 100$ and 500 s are considered. The peak load in all tests was limited to 100 N, which was decided on the basis of trial finite element computations, as explained later. The experiments are repeated for each loading/unloading programme on a new specimen for checking the consistency of the material behaviour. During each of these experiments, the load and displacement data are acquired at a sampling rate of 50/s, which are later filtered to remove undesired noise, and processed for analysis.

Finite element analysis

In this work, axisymmetric simulations of spherical indentation are conducted using the ABAQUS finite element software. In Figure 2, the mesh used in the computations is shown in the r - z plane along with the applied boundary conditions and the indenter (which is taken to be rigid) at incipient contact. The contact between the indenter and the specimen is assumed as frictionless and is modelled using the slideline approach. The mesh shown in Figure 2 is comprised of about 2700 four-noded, isoparametric, quadrilateral elements and is well refined near the zone of indentation. The size of the smallest elements located along the contact surface is around 0.02 mm. This is expected to accurately resolve the steep stress gradients as well as enable precise determination of the contact radius. The dimensions of the domain modelled are five times the radius R of the indenter (see Figure 2) in order to avoid boundary interaction effects.

The material is assumed to obey linear, isotropic viscoelasticity. The experimental relaxation response function $G(t)$ for the PMMA material considered in this work (Figure 1) is employed in the analyses. The maximum time period for which the viscoelastic response is simulated is 1000 s. Since for this duration, it has been demonstrated by Lu *et al.*² that the Poisson ratio ν changes only negligibly, a constant value of $\nu = 0.38$ is assumed. The

analyses are carried out for the two types of load histories employed in the experiments. In both load histories, the peak load is taken as 100 N. This was arrived at on the basis of trial computations using time-independent linear elastic and elastic-plastic material models (wherein experimentally determined quasi-static stress versus strain curve of PMMA was employed). It was found that the load versus displacement curves obtained from these two trial computations agree closely within the above load level, which implies that inelastic effects are minimal.

Results and discussion

In this section, results pertaining to the ramp and hold load history are first presented followed by those for triangular loading. The simulation and analytical results (based on the indentation theories) are compared along with some experimental data. Finally, the creep response function is extracted from the measured displacement history and compared with that deduced from the conventional mechanical test.

The time variations of indentation depth h , contact radius a and peak contact pressure, $p_0 = p(0, t)$ for ramp and hold load history are shown in Figure 3 *a-c*. Here, the analytical results based on the theory of Lee and Radok⁹ (see eqs (3) and (4)) are presented along with those from the numerical analyses. In order to provide further comparison, the measured experimental indentation depth data are plotted in Figure 3 *a*. Here, the mean datapoints

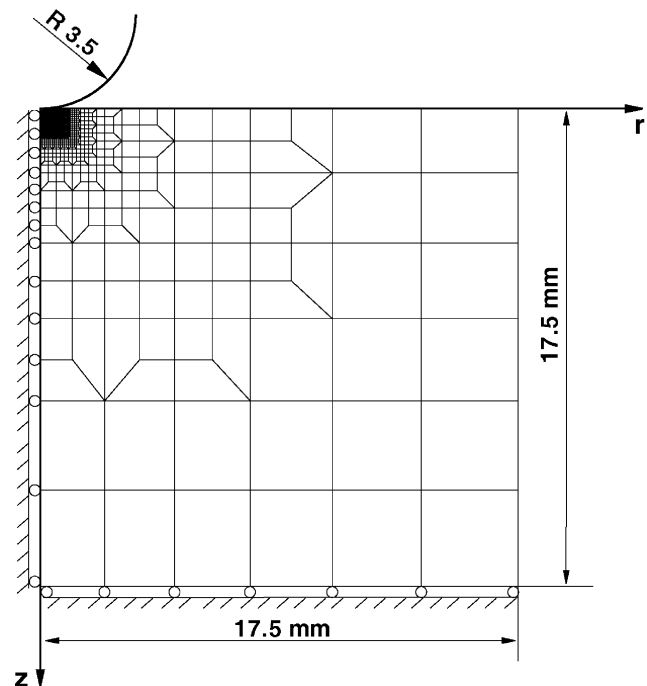


Figure 2. Axisymmetric finite element model used for simulating spherical indentation of a viscoelastic (PMMA) specimen.

(from three tests) are indicated by 'x' symbols and the scatter is shown by bands. Figure 3 a–c demonstrates a close agreement between simulations and the indentation theory. The experimental data for $h(t)$ in Figure 3 a also corroborate well with the analytical variation. It can be

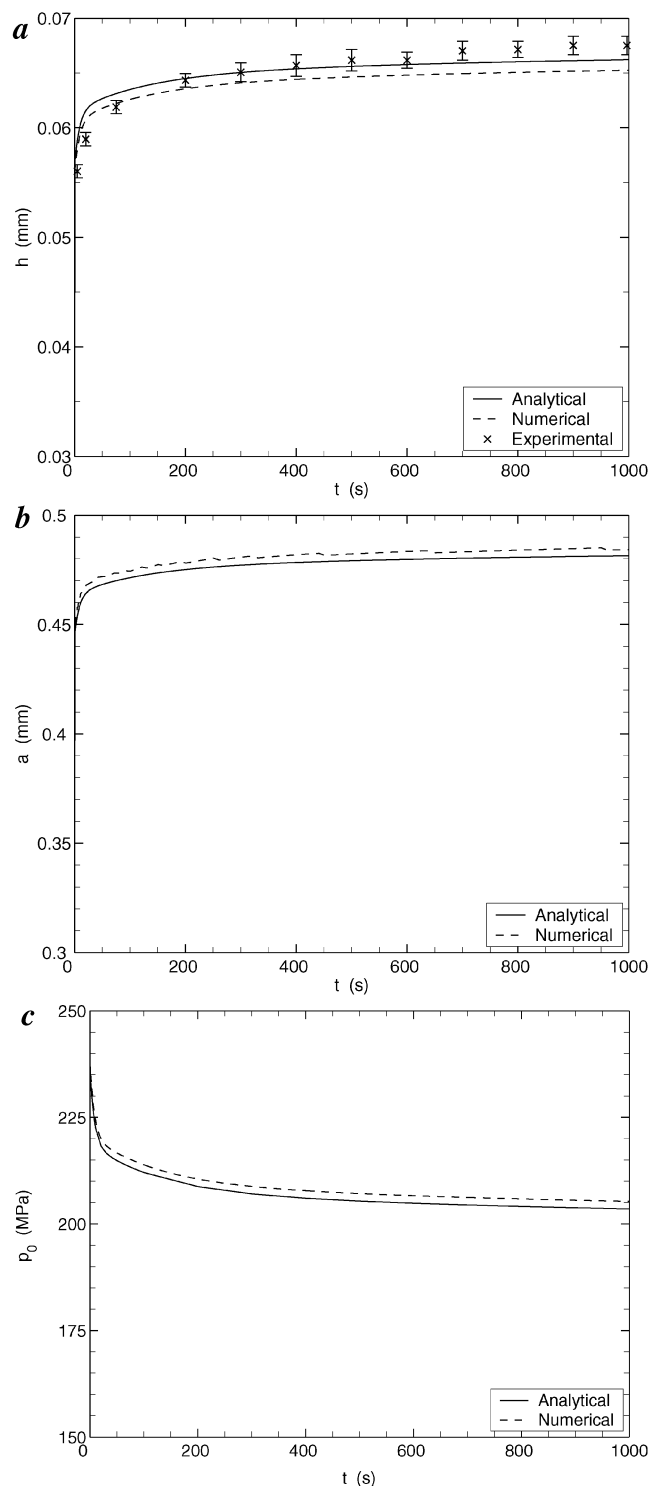


Figure 3. Time variation of (a) indentation depth, (b) contact radius and (c) peak contact pressure for ramp and hold loading history.

seen from Figure 3 a that the indentation depth increases by more than 15% in the time interval from 1 to 1000 s during which the load is held fixed at 100 N. This is due to the creep behaviour of the material.

The time variations of contact radius displayed in Figure 3 b show an increase of about 8% under fixed load over the time duration from 1 to 1000 s. From Figure 3 c, it can be seen that the peak contact pressure decreases with time even though the load is held constant. This drop is quite steep initially and then becomes more gradual. The features discussed above illustrate the viscoelastic response of the material. By contrast, in an elastic material, h , a and p_0 would remain constant under quasi-static conditions when the indentation load is held fixed.

The time variation of contact radius a for triangular loading history with $t_0 = 100$ s, obtained from the analytical solutions of Ting¹² and Lee and Radok⁹ is compared with that determined from finite element analysis in Figure 4. For $t \leq t_0$, $a(t)$ given by the two analytical solutions is the same (see eq. (4)). Figure 4 shows an excellent agreement between Ting's solution and finite element results for the full time range from 0 to $2t_0$ (see solid and dashed line curves). Similar good comparison was found for the other triangular loading histories with $t_0 = 10$ and 500 s. It may be seen from Figure 4 that the contact radius increases to a peak value of around 0.47 mm at $t = t_0$ and thereafter reduces. By contrast, Lee and Radok's solution (represented by the dash-dot curve in Figure 4) differs from the other two curves beyond about 175 s (i.e. $1.75 t_0$) and, in fact, does not reduce to zero at complete unloading. The reason for this discrepancy will be explained later.

In Figure 5 a and b, indentation depth h versus time, and load versus indentation depth are plotted for triangular loading with $t_0 = 10$ s. The analytical solution of Ting¹² is

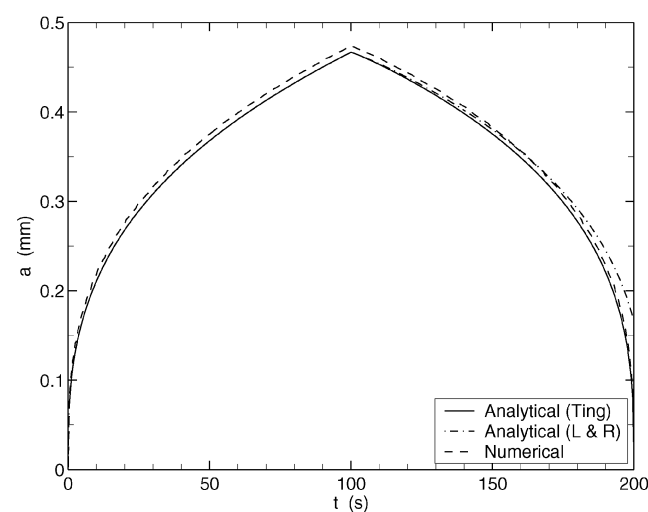


Figure 4. Time variation of contact radius for triangular loading with $t_0 = 100$ s. The analytical solutions proposed by Ting¹², and Lee and Radok⁹ (L&R) are compared with the finite element results.

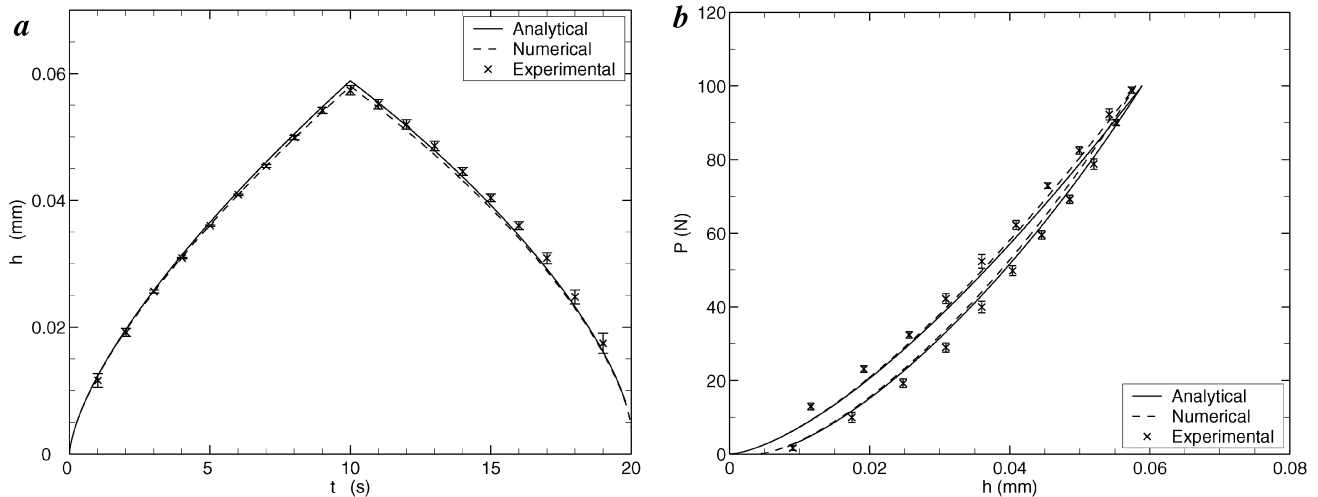


Figure 5. (a) Time variation of indentation depth and (b) load versus indentation depth for triangular loading with $t_0 = 10$ s. The analytical solution of Ting¹² is compared with finite element and experimental results.

Table 1. Values of indentation depth h and contact radius a at peak load obtained from numerical and analytical solutions (eq. (4)) along with experimental data for h_{\max} corresponding to triangular loading histories

t_0 (s)	Displacement h_{\max} (mm)			Contact radius a_{\max} (mm)	
	Numerical	Analytical	Experimental	Numerical	Analytical
10	0.0581	0.059	0.0574	0.461	0.454
100	0.0613	0.0622	0.0615	0.474	0.467
500	0.0634	0.0644	0.0639	0.482	0.475

compared with finite element results as well as with the experimental data. This solution is determined from eq. (4) for $t \leq t_0$ and from eq. (18) for $t > t_0$. In order to evaluate the latter, the contact radius $a(t)$ shown in Figure 4 is employed. Again, an excellent agreement between Ting's solution and finite element as well as experimental results can be perceived in Figure 5a and b. The peak values of h and a (which occur at $t = t_0$) determined from the analytical and finite element solutions for the three triangular loading histories are summarized in Table 1. Also included in Table 1 are average experimental measurements of h_{\max} . The three sets of results for h_{\max} are within 3% of each other. The numerical and analytical results for a_{\max} also agree to within 2%. Further, it can be observed from Table 1 that reduction in loading rate (i.e. increase in t_0), causes increase in h_{\max} and a_{\max} , which is again a characteristic feature of viscoelastic response.

On examining Figure 5b, it can be seen that the loading and unloading curves differ, resulting in some residual depth at complete load removal. This is akin to that exhibited by an elastic-plastic material (see, for example, Bhattacharya and Nix⁶). However, unlike the latter, the residual impression would disappear slowly with time when the viscoelastic specimen is left in the unloaded state. This was indeed observed from the tested speci-

mens and has also been reported by Lu *et al.*⁵. The initial slope of the unloading curve is generally used to obtain the Young's modulus of the material according to the relation⁷:

$$E = \frac{(1-\nu^2)}{2a} \left[\frac{dP}{dh} \right]_{\max} \quad (19)$$

The values of Young's modulus thus extracted from the unloading curve shown in Figure 5b as well as from similar curves for the other two loading rates, are summarized in Table 2 along with those determined from the relaxation response function $G(t)$ (Figure 1) pertaining to the chosen time instants. Also presented in Table 2 are the values of G corresponding to these time instants, which are deduced from the indentation depth measurements as explained below. It can be seen from Table 2 that while the latter are close to those obtained from the conventional relaxation tests, Young's modulus values computed by applying eq. (19) show large errors. In fact, these errors increase with t , attaining almost 50% at $t = 500$ s. Thus, it is clear that the usual interpretation of the initial slope of the unloading curve by employing eq. (19) is incorrect for viscoelastic materials.

Table 2. Values of Young’s modulus corresponding to various time instants obtained from conventional relaxation test and from indentation tests using the traditional method based on unloading slope (eq. (19)) and the method proposed in this work

Time (s)	Young’s modulus (MPa)			
	Conventional relaxation test	Indentation test (from unloading slope)	Indentation ramp test (proposed method)	Indentation ramp and hold (proposed method)
10	2309	2716	2455	2470
100	2141	2850	2229	2190
500	2040	3025	2097	2007

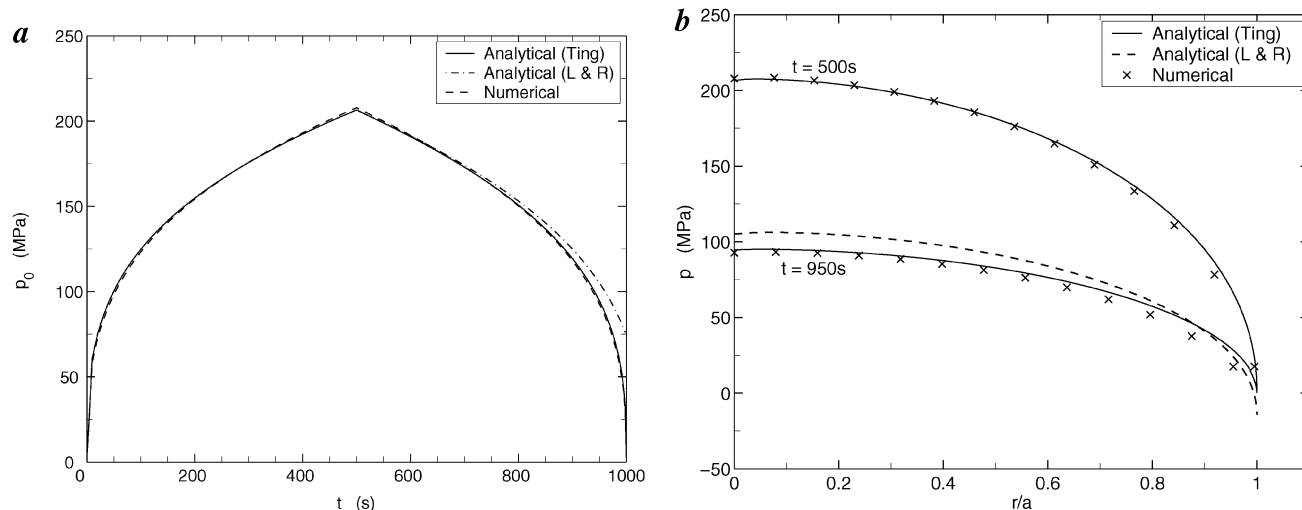


Figure 6. (a) Time variation of peak pressure and (b) contact pressure distribution at two time instants for triangular loading with $t_0 = 500$ s. The analytical solutions proposed by Ting¹² and Lee and Radok⁹ are compared with the finite element results.

Figure 6 a and b shows the time variation of peak pressure $p_0 = p(0, t)$ and the contact pressure distribution corresponding to two time instants for the loading history with $t_0 = 500$ s. Here, the analytical solutions based on Lee and Radok’s theory (eq. (3)) and Ting’s theory (eq. (17)) are compared with the finite element results. As already mentioned, the two analytical solutions coincide for $t \leq t_0$ and also agree well with the finite element solution (see Figure 6 a and b). However, it can be observed from Figure 6 a that while p_0 based on eq. (17) matches closely with the finite element solution even for $t > t_0$, Lee and Radok’s theory (eq. (3)) shows large errors as $t \rightarrow 2t_0$. The reason for this discrepancy can be understood by examining Figure 6 b, which illustrates that while the pressure distribution predicted by eq. (17) over the entire contact zone is positive, that given by eq. (3) becomes negative close to the edge of contact ($r/a = 1$). This leads to the failure of Lee and Radok’s theory to model the unloading behaviour of viscoelastic materials.

The equations for time variation of indentation depth presented earlier, such as eq. (11) for ramp loading (i.e. triangular load history with $t \leq t_0$) or eqs (11) and (12) for ramp and hold loading are fitted to experimentally measured $h(t)$.

To this end, a nonlinear least squares procedure based on the Levenberg–Marquardt algorithm¹⁵ is employed and the Prony series parameters are determined. These are used to reconstruct $J(t)$ from eq. (10). The creep response function thus deduced from the indentation data for $h(t)$ pertaining to ramp and hold test (Figure 3 a) and triangular load history with $t_0 = 500$ s (referred to here as ramp loading) is plotted in Figure 7. Also shown in Figure 7 is $J(t)$ obtained from the conventional mechanical test described earlier. It is clear from Figure 7 that $J(t)$ extracted from the indentation experimental results is in good agreement with that derived from the conventional test. Thus, the instantaneous creep compliance $J(0)$ from the indentation tests is within 7% of that determined from the conventional test, while the long-term compliance (at $t = 1000$ s) agrees to within 3%. Also, the ramp and hold indentation test yields slightly better results than ramp loading.

Finally, it must be noted that relaxation response function $G(t)$ can be obtained by inverting $J(t)$ determined from the indentation tests (i.e. by numerically solving the Volterra integral equation (eq. (6)¹)). The values of G thus computed corresponding to three time instants are presented in Table 2, as mentioned earlier.

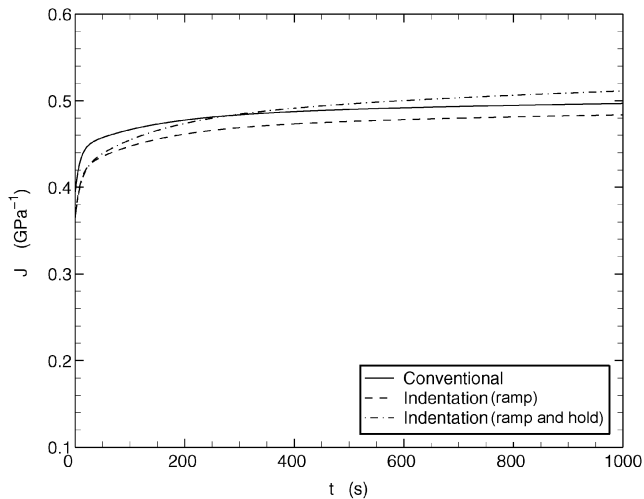


Figure 7. Comparison between creep response function $J(t)$ determined from the indentation tests and conventional mechanical test.

Concluding remarks

Some interesting aspects of time-dependent indentation response of viscoelastic materials are observed from this work. Thus, there is a gradual increase in h and a when the load is held fixed, and h at the same load increases when the loading rate decreases. The finite element results have clearly validated the spherical indentation theory of Ting¹² for linear viscoelastic materials. The experimental data for indentation depth corresponding to ramp and hold, and triangular loading histories, conducted with PMMA specimens, corroborate well with the finite element results and the analytical solution of Ting. Finally, it has been demonstrated that depth-sensing indentation test data can be used to accurately extract the viscoelastic response functions. By contrast, the conventional method based on slope of the unloading curve may lead to large errors in the elastic modulus.

1. Wineman, A. S. and Rajagopal, K. R., *Mechanical Response of Polymers*, Cambridge University Press, Cambridge, UK, 2000.
2. Lu, H., Zhang, X. and Knauss, W. G., Uniaxial, shear, and Poisson relaxation and their conversion to bulk relaxation: Studies on poly(methyl methacrylate). *Polym. Eng. Sci.*, 1997, **37**, 1053–1064.
3. VanLandingham, M. R., Villarubia, J. S., Guthrie, W. G. and Meyers, G. F., Nanoindentation of polymers: An overview. *Macromol. Symp.*, 2001, **167**, 15–43.
4. Sakai, M., Time-dependent viscoelastic relation between load and penetration for an axisymmetric indenter. *Philos. Mag. A*, 2002, **82**, 1841–1849.
5. Lu, H., Wang, B., Ma, J., Huang, G. and Viswanathan, H., Measurement of creep compliance of solid polymers by nanoindentation. *Mech. Time Dependent Mater.*, 2003, **7**, 189–207.
6. Bhattacharya, A. K. and Nix, W. D., Finite element simulations of indentation experiments. *Int. J. Solids Struct.*, 1988, **9**, 881–891.
7. Oliver, W. C. and Pharr, G. M., An improved technique for determining hardness and elastic modulus using load and displacement sensing indentation experiments. *J. Mater. Res.*, 1992, **7**, 1564–1583.
8. Swain, M. V. and Mencik, J., Mechanical property characterization of thin films using spherical tipped indenters. *Thin Solid Films*, 1994, **253**, 204–211.
9. Lee, E. H. and Radok, J. R. M., The contact problem for viscoelastic bodies. *Trans. ASME, J. Appl. Mech.*, 1960, **27**, 438–444.
10. Johnson, K. L., *Contact Mechanics*, Cambridge University Press, Cambridge, UK, 1985.
11. Hunter, S. C., The Hertz problem for a rigid spherical indenter and a viscoelastic half-space. *J. Mech. Phys. Solids*, 1960, **8**, 219–234.
12. Ting, T. C. T., The contact stresses between a rigid indenter and a viscoelastic half-space. *Trans. ASME, J. Appl. Mech.*, 1966, **33**, 845–854.
13. Lee, S. and Knauss, W. G., A note on the determination of relaxation and creep data from ramp tests. *Mech. Time Dependent Mater.*, 2000, **4**, 1–7.
14. Ramesh Kumar, M. V., Experimental and computational studies on spherical indentation of linear viscoelastic solids. M E thesis, Department of Mechanical Engineering, Indian Institute of Science, Bangalore, 2004.
15. Press, W. H., Teukolsky, S. A., Vetterling, W. T. and Flannery, B. P., *Numerical Recipes in FORTRAN*, Cambridge University Press, Cambridge, UK, 1993.

Received 31 July 2004; accepted 5 September 2004